THE JOURNAL OF PHYSICAL CHEMISTRY B

ARTICLE

pubs.acs.org/JPCB

Modeling Self-Diffusion of Simple Fluids in Nanopores

Suresh K. Bhatia* and David Nicholson

School of Chemical Engineering, The University of Queensland, Brisbane, QLD 4072, Australia

ABSTRACT: The recent frictional model of the transport of fluid mixtures in nanopores developed in this laboratory is extended here to formulate a new theory of the self-diffusion of Lennard-Jones fluids in cylindrical pores by considering the problem of diffusion of identical molecules that differ only in color. The new theory is found to predict the self-diffusivity accurately over a wide range of densities and pore sizes, extending from molecularly narrow pores to large mesopores. However, deviations from the theory appear near to the critical temperature where the correlation length of the fluid diverges and when intermolecular interactions are important in molecularly narrow pores. Under such circumstances, local averaging of the fluid−fluid density to obtain a local viscosity does not adequately capture the effects of viscous friction. A new criterion is developed for determining the significance of fluid−fluid intermolecular interactions in a nanopore by considering the ratio of oscillation times of a fluid molecule in the force field of the surrounding fluid molecules and that in the force field of the pore wall. The ratio is shown to give good predictions of the region where intermolecular interactions are important and explains the region of deviation between theory and simulation in molecularly narrow pores.

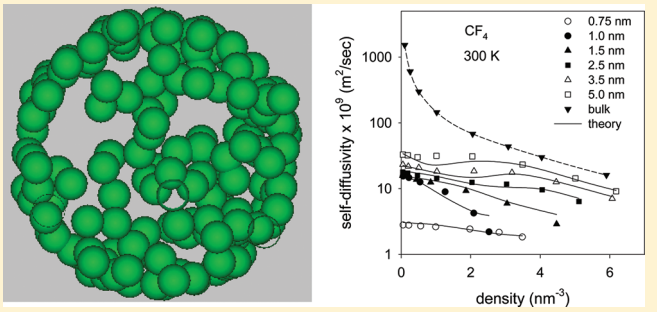

1. INTRODUCTION

The understanding of the transport of fluids in confined spaces has been the subject of attention by researchers for over a century and is of crucial importance for numerous conventional and emerging applications in catalysis, adsorptive and membrane based separations, and electrochemical energy storage. In recent years, there has been a resurgence of interest in the area[1] because of the explosive development of new nanomaterials such as carbon nanotubes,[2] periodic mesoporous silicas,[3] and metal−organic framework materials,[4] as well as a host of others, that have ordered structures with simple and ideal geometry. Such materials are being widely investigated for numerous conventional and novel applications and also provide ideal systems for the development and validation of theories of adsorption and transport. The subject is also of importance to the emerging area of nanofluidics and lab-on-a-chip technology[5] and to biological systems such as the transport in aquaporins and membrane protein channels.[6]

It is now well understood[7] that there are two modes of diffusion in confined spaces. The most commonly investigated of these is transport diffusion, which represents the motion of the center of mass of the fluid and is governed by collective behavior.[8−10] The other is the tracer or self-diffusion coefficient, which characterizes the response of a single particle (a "tracer" molecule) to other fluid particles and the confining pore walls.[8−13] Macroscopic measurements of transport coefficients based on uptake rates in porous adsorbent particles or the flux through membranes are representative of the motion of the fluid as a whole and yield the collective or transport diffusivity. On the other hand, microscopic measurements using pulse field gradient nuclear magnetic resonance (PFG-NMR) or quasi-elastic neutron scattering (QENS) techniques are affected by individual particle relaxation behavior and yield the self-diffusivity.[7,14−16] In both cases, the flux follows the phenomenological model

$$j = \frac{D_0 \rho}{R_g T}(-\nabla \mu) \tag{1}$$

where $(-\nabla\mu)$ represents the chemical potential driving force of the diffusing species and ρ its molecular density. In the case of transport diffusion, the coefficient D_0 is commonly termed the corrected diffusivity, denoted D_{t0}, while in the case of self-diffusion it represents the intrinsic mobility or self-diffusivity, D_{s0}. A notable difference between D_{t0} and D_{s0} is that, whereas the former increases with density because of the combined effects of diffusive and viscous-like flow,[1,8−10] the self-diffusivity, D_{s0}, generally decreases strongly with an increase in density.[8] Although this is usually the case for single nanopores and homogeneous systems, on the basis of simulation evidence,[8] PFG-NMR experiments with disordered nanoporous materials have yielded a maximum in the self-diffusivity with an increase in density,[17] which may well be due to pore size distribution effects, with larger pores that offer higher diffusivity increasing in contribution and leading to the maximum. Such effects have been discussed earlier by Kärger and Ruthven,[7] who note that in the presence of heterogeneity, the

Received: July 17, 2011
Revised: September 6, 2011
Published: September 08, 2011

self-diffusivity can increase with an increase in density because the molecules on initially occupied sites are more strongly adsorbed and have lower mobility than those adsorbed at higher densities. Techniques for analyzing such occupancy effects and those of pore topology have been developed by Coppens et al. using Monte Carlo simulations on lattice models.[18] At low density, when intermolecular interactions are negligible, the two coefficients (i.e., the corrected and self-diffusivities) are expected to be equal to each other.[8] However, there is some evidence from simulation that this is not necessarily the case for rough surfaces, in which molecules trapped within local pockets influence the self-diffusivity but do not contribute to transport diffusion.[19,20]

Although a theory to predict the corrected diffusivity associated with actual transport has received much attention in recent years,[1] accurate and tractable models for predicting the self-diffusivity in nanomaterials from molecular properties alone have received much less interest. The dusty gas model (DGM)[21] remains the most popular approach for predicting pore as well as macroscopic fluxes in pore networks (through incorporation of a tortuosity). However, the model has been criticized[1] because it invokes conflicting choices of frames of reference in its derivation and because it relies on the Knudsen model to describe diffusion at low densities. It has been shown[22−25] that the Knudsen model, being based on a hard sphere molecular model that omits attractive wall interactions, can overpredict the low density diffusion coefficient, calculated from molecular dynamics simulations, by as much as a factor of 10. This problem with the Knudsen model has also been the subject of attention by Krishna and co-workers,[26,27] who find that it overpredicts molecular dynamics simulation results for the low density diffusion coefficients by an order of magnitude. The Maxwell−Stefan analysis of Krishna[28,29] implicitly allows for the adsorbent force field through the use of empirical pure component diffusion coefficients in modeling mixture behavior. Rigorous statistical mechanical approaches based on the kinetic theory of dense fluids have been developed[30−32] but have essentially proved intractable due to the large number of degrees of freedom involved when modeling multiparticle systems. In addition, they rely on contact pair distributions that must be obtained by molecular dynamics simulation and are therefore not fully predictive. The agreement with simulation is also modest, with errors as large as 60% in some cases.[11] Other recent treatments by Guo and co-workers[33,34] and Marconi and Melchionna[35] have used the Boltzmann equation with the Bhatnagar−Gross−Krook (BGK) approximation[36] for the collision term. However, the BGK approximation is at best semiempirical because it uses a relaxation time, taken as the reciprocal of the collision frequency. This may not be accurate in nanopores where strong density gradients exist and the mean free path is comparable to the pore size. Moreover, the mean free path and consequently collision frequency are ill-defined concepts for continuous interaction potentials. Kharat et al.[13] used a memory kernel formulation to derive a hierarchy of coupled integro-differential equations for the velocity autocorrelation function, which yields the low-density self-diffusivity in NaY zeolite. The solution requires a closure approximation that in general may not be known a priori. Predicting the behavior at finite density requires further development.

A more promising approach for predicting transport coefficients of pure components and mixtures is the friction based model of Bhatia and co-workers,[1,37,38] which considers the wall effect via a friction coefficient that is related to the low density transport coefficient. The low density transport coefficient is predicted from first principles by the exact oscillator model of Bhatia and co-workers,[22,23] in which the trajectory time of a fluid particle oscillating between diffuse collisions with the pore walls is calculated from the equations of motion. The frictional model utilizes a microscopic momentum balance based on the Bearman−Kirkwood theory for bulk fluids,[39] with an added friction term to account for momentum loss in the direction of transport due to wall collision occurring in the region beyond the location of the fluid−solid potential minimum. The approach has been validated against molecular dynamics simulations for single component transport coefficients and for Onsager coefficients in multicomponent transport and offers an attractive option for predicting self-diffusion coefficients in nanopores. The method is also computationally faster than molecular dynamics (MD) simulations by at least 2 orders of magnitude and is accurate at all densities in mesopores. Here we develop a theory of self-diffusion in nanopores based on the same approach, which is shown to be in very good agreement with exact MD results over a wide range of pore sizes and densities. A new criterion is developed for the onset of significant fluid−fluid interactions in a nanopore, at which point viscous interactions become important and influence the transport.

2. THEORY

2.1. Self-Diffusion in a Cylindrical Nanopore. The starting point of the present theory for self-diffusion is the microscopic momentum balance[37,38]

$$\frac{1}{r}\frac{\mathrm{d}}{\mathrm{d}r}\left(r\eta_i\frac{\mathrm{d}\overline{v}_i}{\mathrm{d}r}\right) = \rho_i(r)\frac{\mathrm{d}\mu_i}{\mathrm{d}z} + \rho_t(r)k_\mathrm{B}T\sum_{j=1}^{n}\frac{x_i x_j(\overline{v}_i-\overline{v}_j)}{D_{ij}} + \xi_i\rho_i\overline{v}_i a(r-r_{0i}) \quad (2)$$

for species i with axial component of the streaming velocity $\overline{v}_i$, for a mixture, in a cylindrical nanopore of radius r_p measured between the cylinder axis and the atom centers in the first annulus of adsorbent. ξ_i is a uniformly distributed wall friction coefficient for species i, such that the last term on the right-hand side of eq 2 represents the rate of momentum loss due to molecule wall collisions in the repulsive region of the fluid−solid interaction potential, $r_{0i} < r < r_\mathrm{p}$, where r_{0i} represents the location of the minimum of the fluid solid potential for species i and $a(r - r_{0i})$ is the Heaviside function having the value of unity for $r > r_{0i}$ and zero otherwise. The coefficient η_i represents a partial viscosity, related to the mixture viscosity (η) by[37,38] $\eta_i = \omega_i\eta$, where ω_i is the weight fraction of species i. In utilizing a species specific partial viscosity, eq 2 differs from the conventional reference frame based on the mixture averaged velocity, embodied in the Enskog derivation of the transport coefficients.[40] The approach based on the mixture averaged velocity has been criticized[41] on the grounds that the expansion of the individual species velocities around the mixture average in the Enskog treatment may not converge when the mobilities of the individual species are widely different.

Equation 2 is based on the Newtonian shear stress model, whose validity has been questioned for nonuniform fluids, and an empirical nonlocal model based on generalized hydrodynamics has instead been suggested.[42] However, an expression in terms of molecular parameters for the nonlocal viscosity kernel is still not available. An alternative formulation that allows for nonlocality, albeit retaining the Newtonian description, is the local averaged density model (LADM) of Bitsanis et al.,[43] in which the viscosity is estimated at a coarse-grained density, locally averaged over a sphere of molecular dimensions as

$$\tilde{\rho}_i(\mathbf{r}) = \frac{6}{\pi\sigma_{\mathrm{ff},i}^3}\int_{|\mathbf{r}'|<1/2\sigma_{\mathrm{ff},i}} \rho_i(\mathbf{r}+\mathbf{r}')\,\mathrm{d}\mathbf{r}' \tag{3}$$

where σ_{ff} is the Lennard-Jones (LJ) size parameter of the fluid particles. The LADM has been fruitfully exploited by us[9,10,23,37,38] to determine the corrected diffusion coefficient of LJ fluids in cylindrical silica and slit pores. The success of this approximation is largely because the region where the bulk-viscosity based LADM is least accurate is that of low density, where fluid intermolecular collisions are infrequent and the viscous contribution is negligible. At high density, as the viscous contribution increases, the LADM becomes more accurate.

When the corrected diffusivity is to be determined for a pure component, the mutual diffusion (second) term on the right-hand side of eq 2 is absent, and the equation may be solved using the equilibrium density profile $\rho(r)$ obtained from grand canonical Monte Carlo (GCMC) simulation or density functional theory; it has been shown[9,10,23] that equilibrium density profiles are maintained even during transport driven by a force field. Equation 1 represents a boundary value problem for the streaming velocity profile, $\overline{v}(r)$, with boundary conditions $\mathrm{d}\overline{v}(r)/\mathrm{d}r = 0$ at $r = 0$ and $r = r_{\mathrm{p}}$. The first of these represents the usual symmetry condition, whereas the second reflects the fact that at the center-line of the solid surface, i.e., at $r = r_{\mathrm{p}}$, the fluid density and hence shear stress must decay to zero. The flux is then obtained from the velocity profile, $v(r)$, following

$$j = \frac{2}{r_{\mathrm{p}}^2}\int_0^{r_{\mathrm{p}}} r\rho(r)v(r)\,\mathrm{d}r \tag{4}$$

To derive the new model of the self-diffusion in a cylindrical nanopore starting from eq 2, we consider the color diffusion problem in a binary mixture of otherwise identical species in a cylindrical nanopore. In such a case, the mole fraction and weight fraction for each species are identical, and eq 2 reduces to

$$\frac{1}{r}\frac{\mathrm{d}}{\mathrm{d}r}\left(rx_i\eta(\tilde{\rho}_{\mathrm{t}}(r))\frac{\mathrm{d}\overline{v}_i}{\mathrm{d}r}\right) = x_i\rho_{\mathrm{t}}(r)\frac{\mathrm{d}\mu_i}{\mathrm{d}z} + \rho_{\mathrm{t}}(r)k_{\mathrm{B}}T\sum_{j=1}^{n}\frac{x_ix_j(\overline{v}_i-\overline{v}_j)}{D_{ii}(\tilde{\rho}_{\mathrm{t}}(r))} + \xi_ix_i\rho_{\mathrm{t}}(r)\overline{v}_ia(r-r_{0i}),\quad i=1,2 \tag{5}$$

because $\eta_i = \omega_i\eta$. Here, $\rho_{\mathrm{t}}(r)$ is the total density. Because the diffusing species are identical except for their color, separative forces are absent, and the mole fraction x_i is independent of radial position. Further, for the color diffusion problem, there is no net flux of the mixture, and

$$x_1\overline{v}_1(r) + x_2\overline{v}_2(r) = 0 \tag{6}$$

With x_i independent of r, eqs 5 and 6 combine to yield, for either species,

$$\frac{1}{r}\frac{\mathrm{d}}{\mathrm{d}r}\left(r\eta(\tilde{\rho}_{\mathrm{t}}(r))\frac{\mathrm{d}\overline{v}_i}{\mathrm{d}r}\right) = \rho_{\mathrm{t}}(r)\frac{\mathrm{d}\mu_i}{\mathrm{d}z} + \frac{k_{\mathrm{B}}T\rho_{\mathrm{t}}(r)\overline{v}_i}{D_{11}(\tilde{\rho}_{\mathrm{t}}(r))} + \xi_i\rho_{\mathrm{t}}\overline{v}_ia(r-r_{0i}),\quad i=1,2 \tag{7}$$

where $D_{11} = D_{22}$ is the bulk self-diffusivity. Clearly, the friction coefficient ξ_i is the same for each species. Upon solving eq 7 with the boundary conditions discussed above, the self-diffusivity in the nanopore is obtained by combining it with eq 1, as

$$D_{\mathrm{s0}}(\hat{\rho}_{\mathrm{t}}) = \frac{2k_{\mathrm{B}}T}{r_{\mathrm{p}}^2\hat{\rho}_{\mathrm{t}}}\int_0^{r_{\mathrm{p}}} r\rho_{\mathrm{t}}(r)\left(\frac{\overline{v}_i(r)}{(-\nabla\mu_i)}\right)\mathrm{d}r \tag{8}$$

where $\hat{\rho}_{\mathrm{t}}$ is the mean total fluid density in the nanopore, given by

$$\hat{\rho}_{\mathrm{t}} = \frac{2}{r_{\mathrm{p}}^2}\int_0^{r_{\mathrm{p}}} r\rho(r)\,\mathrm{d}r \tag{9}$$

and the flux $j_i(r) = \rho_i(r)\overline{v}_i(r)$.

The bulk viscosity, $\eta(\rho)$, and self-diffusivity, $D_{11}(\rho)$, may be obtained by MD simulations for the pure bulk fluid, whereas the total density profile, $\rho_{\mathrm{t}}(r)$, may be obtained from GCMC simulation or density functional theory. MD simulation-based correlations for the bulk viscosity and self-diffusivity exist for LJ fluids[44,45] and have been employed by us earlier.[37,38] However, the accuracy of such correlations is within about 20%, and in the present work, we have determined the bulk viscosity and self-diffusivity by MD simulation.

For LJ fluids, the friction coefficient, ξ_i, is related to the low density diffusion coefficient D_{0i}^{LD} by[37,38]

$$\xi_i = -\frac{k_{\mathrm{B}}T\int_0^{r_{\mathrm{p}}} r\mathrm{e}^{-\phi_{\mathrm{fs},i}(r)/k_{\mathrm{B}}T}\,\mathrm{d}r}{D_{0i}^{\mathrm{LD}}\int_{r_{0i}}^{r_{\mathrm{p}}} r\mathrm{e}^{-\phi_{\mathrm{fs},i}(r)/k_{\mathrm{B}}T}\,\mathrm{d}r} \tag{10}$$

and a separate theory,[22,23] termed the oscillator model, has been developed to determine the low density diffusivity from molecular parameters. According to this theory, for particles that are diffusely reflected from the pore walls, the low density diffusivity is given by

$$D_0^{\mathrm{LD}} = \frac{k_{\mathrm{B}}T}{m}\langle\tau\rangle \tag{11}$$

where $\langle\tau\rangle$ is the mean travel time of a trajectory between diffuse reflections. The travel time of a trajectory is obtained by solving the equations of motion of a fluid particle of given energy under the action of the fluid−solid potential, and the mean time $\langle\tau\rangle$ is obtained as the canonical average of the travel times. For a fluid particle confined in a cylindrical space and having radial and angular momenta, p_{r} and p_θ, respectively, at some position r, the trajectory time is obtained as

$$\tau(r,p_{\mathrm{r}},p_\theta) = 2m\int_{r_{\mathrm{c0}}(r,p_{\mathrm{r}},p_\theta)}^{r_{\mathrm{c1}}(r,p_{\mathrm{r}},p_\theta)}\frac{\mathrm{d}r'}{p_{\mathrm{r}}(r',r,p_{\mathrm{r}},p_\theta)} \tag{12}$$

where $p_r(r', r, p_r, p_\theta)$ is its radial momentum when it is at radial position r' and is given by

$$p_r(r', r, p_r, p_\theta) = \left(2m\left[\phi_{fs}(r) - \phi_{fs}(r')\right] + \frac{p_\theta^2}{r^2}\left[1 - \left(\frac{r}{r'}\right)^2\right] + p_r^2(r)\right)^{1/2} \tag{13}$$

and r_{c0} (r, p_r, p_θ) and r_{c1} (r, p_r, p_θ) are the radial bounds of the trajectory obtained from $p_r(r', r, p_r, p_\theta) = 0$. Here, the angular momentum, being conserved in the absence of tangential forces, is constant along a trajectory. Here, $\phi_{fs}(r)$ is the fluid-wall potential field. Equations 11−13 combine to yield

$$D_0^{LD} = \frac{2}{\pi m Q}\int_0^\infty e^{-\beta\phi_{fs}(r)}\,dr \int_0^\infty e^{-\beta p_r^2/2m}\,dp_r \times \int_0^\infty e^{-\beta p_\theta^2/2mr^2}\,dp_\theta \int_{r_{c0}}^{r_{c1}} \frac{dr'}{p_r(r', r, p_r, p_\theta)} \tag{14}$$

where $\beta = (k_B T)^{-1}$ and $Q = \int_0^\infty r e^{-\beta\phi_{fs}(r)}\,dr$. Equations 7−14 complete the model of self-diffusion in a nanopore. We note here that a frictional model, also invoking fractional species viscosities, has been proposed by Kerkhof[46] but relies on the use of the hard sphere interaction-based Knudsen diffusivity in determining the wall friction coefficient. The latter has been shown[22,23] to overpredict the diffusion coefficient in the presence of van der Waals interactions between the fluid and pore wall.

2.2. Criterion for Significance of Fluid−Fluid Interactions. As mentioned earlier, the use of the LADM has proved successful because its region of inaccuracy is the low density region of insignificant fluid−fluid intermolecular interactions. Nevertheless, in narrow nanopores of molecular dimensions, the issue is further complicated by the low-dimensional nature of the transport. In such pores, the bulk-based viscosity, reflecting the three-dimensionally symmetric nature of the bulk fluid, may be inaccurate. In this circumstance, it is likely that the LADM will be inaccurate even in the presence of strong fluid−fluid intermolecular interactions and at high densities. It is therefore of interest to develop a criterion for testing the significance of these interactions in a nanopore. To this end, we consider the oscillation of a fluid molecule slightly perturbed from its equilibrium position in the force field of the surrounding molecules in the pore. Intermolecular interactions are important when the period of this oscillation is comparable to or smaller than that of the radial oscillation in the force field of the pore wall (i.e., $\langle\tau\rangle$). In this case, molecules oscillating in the wall force field will "feel" the influence of other molecules.

The intermolecular force on a fluid particle located at radial position r in a cylindrical nanopore is given by

$$\mathbf{F}(r) = \int \left[-\nabla\phi_{ff}(|\mathbf{r} - \mathbf{r}'|)\right] g(|\mathbf{r} - \mathbf{r}'|)\rho(r')\,d\mathbf{r}' \tag{15}$$

where $\phi_{ff}(|\mathbf{r} - \mathbf{r}'|)$ is the intermolecular potential energy of interaction between a molecule located at $\mathbf{r}$ and another at $\mathbf{r}'$ and $g(|\mathbf{r} - \mathbf{r}'|)$ is the corresponding pair distribution function. The axial component of this force is

$$F_z = \int_{-\infty}^\infty \int_0^{2\pi} \int_0^{r_p} \left(-\frac{d\phi_{ff}}{db}\right)\frac{\partial b}{\partial z} g(b)\rho(r')r'\,dr'\,d\theta'\,dz \tag{16}$$

where $b\,(= |\mathbf{r} - \mathbf{r}'|)$ is the distance between the two molecules. In polar coordinates, this distance is given by

$$b(r, z, r', \theta') = \sqrt{\left[r^2 + r'^2 - 2rr'\cos(\theta') + z^2\right]} \tag{17}$$

where z is the axial separation between the molecules. At equilibrium, the net force on the particle at $\mathbf{r}$ is zero; however, a small displacement of this molecule will lead to its localized oscillations within the force field of the surrounding molecules. We now consider a small axial displacement, $\tilde{z}$, of the molecule originally at equilibrium at radial position r, while considering the surrounding molecules to remain at their original positions. To the first order in the perturbation, the axial force on the oscillating molecule is then given by

$$\begin{aligned} -F_z &= \int_{-\infty}^\infty \int_0^{2\pi} \int_0^{r_p} \left[\left(\frac{d\phi_{ff}}{db}\right)_{eq} + \tilde{z}\left(\frac{d^2\phi_{ff}}{db^2}\right)_{eq}\left(\frac{\partial b}{\partial z}\right)_{eq}\right] \\ &\quad \times \left[\left(\frac{\partial b}{\partial z}\right)_{eq} + \tilde{z}\left(\frac{\partial^2 b}{\partial z^2}\right)_{eq}\right] g(b)\rho(r')r'\,dr'\,d\theta'\,dz \\ &= \tilde{z}\int_{-\infty}^\infty \int_0^{2\pi} \int_0^{r_p} \left[\left(\frac{d^2\phi_{ff}}{db^2}\right)_{eq}\left(\frac{\partial b}{\partial z}\right)_{eq}^2 + \left(\frac{d\phi_{ff}}{db}\right)_{eq}\left(\frac{\partial^2 b}{\partial z^2}\right)_{eq}\right] \\ &\quad \times g(b)\rho(r')r'\,dr'\,d\theta'\,dz \\ &= A\tilde{z} \end{aligned} \tag{18}$$

where

$$A = 2\int_0^\infty \int_0^{2\pi} \int_0^{r_p} \left[\left(\frac{d^2\phi_{ff}}{db^2}\right)_{eq}\left(\frac{z}{b}\right)^2 + \left(\frac{d\phi_{ff}}{db}\right)_{eq}\left(\frac{b^2 - z^2}{b^3}\right)\right] g(b)\rho(r')r'\,dr'\,d\theta'\,dz \tag{19}$$

A simple force balance on the displaced molecule originally at r provides

$$m\ddot{\tilde{z}} + A\tilde{z} = 0 \tag{20}$$

which yields its oscillation period under the action of fluid−fluid intermolecular forces

$$\tau_m(r) = \frac{2\pi}{\sqrt{A/m}} = \frac{\pi\sqrt{2m}}{\left(\int_0^\infty \int_0^{2\pi} \int_0^{r_p} \left[\left(\frac{d^2\phi_{ff}}{db^2}\right)_{eq}\left(\frac{z}{b}\right)^2 + \left(\frac{d\phi_{ff}}{db}\right)_{eq}\left(\frac{b^2 - z^2}{b^3}\right)\right] g(b)\rho(r')r'\,dr'\,d\theta'\,dz\right)^{1/2}} \tag{21}$$

dx.doi.org/10.1021/jp206811a |J. Phys. Chem. B 2011, 115, 11700–11711

Table 1. Fluid−Fluid LJ Interaction Parameters

fluid parameter	CH_4	CF_4	CCl_4
σ_{ii} (nm)	0.381	0.4662	0.5947
ϵ_{ii}/k_B (K)	148.1	134	322.7

Intermolecular forces will have significant influence when, for any radial position r, the value of $\tau_m(r)$ is not much larger than the period, $\langle\tau\rangle$, of the oscillation under the influence of the pore wall potential.

2.3. Potential Energy. Whereas the above approach is quite general and can accommodate any pore wall−fluid potential, in the present work we have used the Tjatjopoulos et al.[47] potential

$$\phi_{fs}(r) = 16\varepsilon_{fs}\rho_s r_p \int_0^\infty dz \int_0^\pi \left[\left(\frac{\sigma_{fs}}{r'}\right)^{12} - \left(\frac{\sigma_{fs}}{r'}\right)^{6}\right] d\alpha \tag{22}$$

which considers the pore surface to comprise randomly distributed sites interacting with LJ fluid particles by a LJ 6−12 potential. Here, $r' = (z^2 + r^2 + r_p^2 - 2rr_p\cos(\alpha))^{1/2}$, ε_{fs}, and σ_{fs} are fluid−solid Lennard-Jones parameters, and ρ_s is the areal density of pore surface sites. The pore wall is considered to be composed of disordered silica and comprises a single layer whose interaction with a fluid molecule is modeled through eq 22. For a silica surface, the interaction is assumed to be dominated by a surface layer of oxygen atoms, having potential parameters $\varepsilon_{00}/k_B = 492.7$ K, $\sigma_{00} = 0.28$ nm, with $\rho_0 = 10.47$ nm^{-2} based on the results of Neimark et al.[48] Fluid−solid potential parameters were estimated using the Lorentz−Berthelot rules. Table 1 lists the fluid−fluid potential energy parameters used.

3. SIMULATION

GCMC and equilibrium molecular dynamics (EMD) simulations have been performed here, using methane at 200, 300, and 400 K as well as CF_4 and CCl_4 at 300 K, modeled as LJ fluids, in cylindrical pores in amorphous silica, using the potential model outlined above. Various pore sizes covering the range of 0.75−5 nm diameter were chosen for the simulations. The GCMC simulations were conducted to obtain pair distribution functions of the adsorbate at various densities in the nanopore. These simulations used the standard Adams[49] scheme, comprising trials of three types: moving a molecule, creating a molecule, and deleting a molecule. The probability of a move being accepted was evaluated by using the Metropolis sampling scheme.[50] In the simulations, a cutoff distance for potential energy calculations of 1.5 nm was used for CH_4, whereas for CF_4 and CCl_4, the cutoff distance was 2.5 and 3 nm, respectively. Each simulation run sampled a total of 10^7 configurations, of which the first 10^5 were rejected in calculating averages. The pore lengths were to chosen to ensure about 250 particles in the pore.

In the equilibrium molecular dynamics simulations, a fixed number of particles, volume, and temperature (NVT) ensemble was used, and the trajectories of methane molecules in the pore were tracked using the equation of motion. Each run started from an arbitrary initial configuration having about 250 particles, generated using GCMC simulation at a chosen chemical potential. The Gaussian thermostatting technique[51] was employed for efficient temperature control, as it provides a rigid constraint on the kinetic energy. A fifth order Gear predictor−corrector method with a time step of 1−2 fs was used to solve the equations of motion. The run-length was typically about 10^7 steps, of which the first 10^6 steps were rejected. Cut-off distances were the same as those given above. Particles were considered to be diffusely scattered in the osculating plane at the pore wall, so that on reflection the axial and angular components of the velocity are randomized, while maintaining detailed energy balancing. A reflection occurs when, while moving toward the wall, the radial component of the velocity of the particle is reversed, and it is closer to the wall than the minimum of the fluid−solid potential. From the EMD simulations, the self-diffusivity was determined from the autocorrelation of the individual particle velocities via a Green−Kubo relation[8,52]

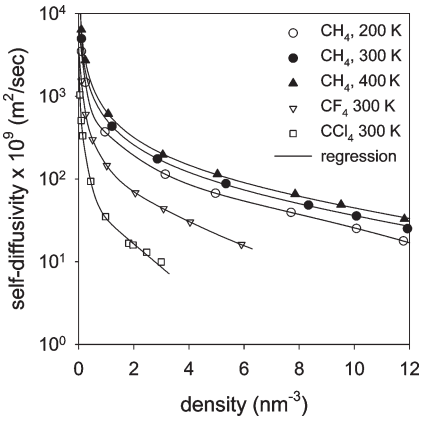

Figure 1. Variation of bulk self-diffusivity with density.

$$D_{s0} = \frac{1}{N}\lim_{\tau\to\infty}\sum_{i=1}^{N}\int_0^\tau \langle v_{iz}(t)v_{iz}(0)\rangle\, dt \tag{23}$$

Density profiles were also obtained from the EMD simulations, with the position data for the first 10^6 time steps rejected.

We note here that the condition of diffuse reflection at the wall is similar to that embedded in the Knudsen model of low density diffusion in hard sphere systems and essentially assumes thermalization of the reflected molecules at a rigid wall. Thus, successive trajectories of a molecule are uncorrelated, and this assumption has been used in the derivation of the oscillator model.[22,23] This idealized diffuse reflection model is not necessarily a precise representation of a real solid wall, as simulations using atomically detailed models of solid surfaces, such as those of defect-free carbon nanotubes, reveal close to specular reflection with a nearly frictionless flow of adsorbed molecules.[53−55] However, the surfaces of real solids are rarely defect free, and the reflection can have a very significant diffuse component in the presence of surface roughness.[56] Indeed, the diffusivities of molecules in activated carbons and zeolites are typically[7] in the range of 10^{-12}−10^{-8} m^2/s, several orders of magnitude lower than those in ideal carbon nanotubes and in the range of values predicted for diffuse reflection,[24] indicating that this is a reasonable approximation for real surfaces, which are imperfect and whose atomistic structure is not well-defined. Even otherwise, the boundary condition may be readily adapted[55] for partially specular reflection by considering the Smoluchowski correction based on the Maxwell reflection coefficient.

To determine bulk self-diffusivities and viscosities for use in the model of Section 2.1, EMD simulations were performed for the bulk fluid at various densities, in a manner similar to that for the pore fluid discussed above. A cubic simulation box was taken,

Table 2. Correlation of Bulk Self-Diffusivity for Different Fluids

fluid	temperature (K)	self-diffusivity, $D_{s0} \times 10^9$ (m^2/s)
CH_4	200	$6397e^{-8.191\rho} + 1625.79e^{-0.946\rho} + 142.45e^{-0.138\rho} - 10.41$
		$0.1 < \rho < 11.8$ nm^{-3}
CH_4	300	$571.20/\rho - 26.96/\rho^2 + 2.15/\rho^3 - 20.73$
		$0.1 < \rho < 11.9$ nm^{-3}
CH_4	400	$686.22/\rho - 5.056/\rho^2 + 0.0629/\rho^3 - 23.883$
		$0.1 < \rho < 11.8$ nm^{-3}
CF_4	300	$4.604 + 3004.21e^{-11.482\rho} + 597.39e^{-2.493\rho} + 145.03e^{-0.43\rho}$
		$0.1 < \rho < 5.9$ nm^{-3}
CCl_4	300	$2159.06e^{-31.174\rho} + 599.28e^{-5.691\rho} + 59.91e^{-0.648\rho}$
		$0.05 < \rho < 3$ nm^{-3}

Table 3. Correlation of Bulk Shear Viscosity for Different Fluids

fluid	temperature	viscosity, η (mPa·s)
CH_4	200 K	$7.033 \times 10^{-3}e^{0.127\rho} + 1.201 \times 10^{-4}e^{0.435\rho}$
		$0.1 < \rho < 11.8$ nm^{-3}
CH_4	300 K	$9.13 \times 10^{-3} + 1.87 \times 10^{-3}\rho - 1.41 \times 10^{-4}\rho^2 + 2.48 \times 10^{-5}\rho^3$
		$0.1 < \rho < 11.9$ nm^{-3}
CH_4	400 K	$0.014 + 8.84 \times 10^{-4}\rho + 4.29 \times 10^{-6}\rho^2 + 1.92 \times 10^{-5}\rho^3$
		$0.1 < \rho < 11.8$ nm^{-3}
CF_4	300 K	$0.017 + 1.39 \times 10^{-3}\rho + 5.63 \times 10^{-4}\rho^2 + 8.65 \times 10^{-5}\rho^3$
		$0.1 < \rho < 5.9$ nm^{-3}
CCl_4	300 K	$(9.13 \times 10^{-3} - 0.0144\rho + 0.0173\rho^2)/(1 - 0.968\rho - 2.465 \times 10^{-3}\rho^2 + 0.171\rho^3)$
		$0.05 < \rho < 3$ nm^{-3}

of a size large enough to accommodate about 250 particles at each density, which was found large enough to yield a sample-size-independent diffusion coefficient. The bulk self-diffusivity was estimated from the molecular trajectories using

$$D_{s0,\text{bulk}} = \frac{1}{3N}\lim_{\tau\to\infty}\sum_{i=1}^{N}\int_0^\tau \langle \mathbf{v}_i(t)\cdot\mathbf{v}_i(0)\rangle \, dt \quad (24)$$

whereas the bulk fluid shear viscosity was determined using the stress autocorrelation function, following the Green−Kubo relation

$$\eta = \frac{V}{3k_B T}\lim_{\tau\to\infty}\sum_{\alpha<\beta}^{N}\int_0^\tau \langle \Pi_{\alpha\beta}(t)\Pi_{\alpha\beta}(0)\rangle \, dt \quad (25)$$

where Π is the stress tensor.

4. RESULTS AND DISCUSSION

4.1. Bulk Simulations. Initially, EMD simulations were performed for the bulk fluid, as discussed above, to determine the self-diffusivity and viscosity of the various gases as a function of density for use in the theory. The results of these simulations were regressed in the form of simple correlations that can be readily used. Figure 1 depicts the density variation of the self-diffusivity of bulk CH_4 at 200, 300, and 400 K and of CF_4 and CCl_4 at 300 K. On the basis of several repeat runs with different starting configurations, the error of the simulations is within 5%, and the error bars are smaller than the size of the symbols in Figure 1. The solid lines in the figure depict the correlations that resulted from regressions of the simulation data. Table 2 lists the correlations obtained.

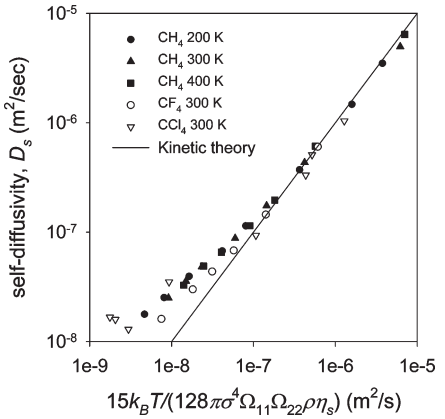

Figure 2. Correlation between self-diffusivity and viscosity based on EMD results.

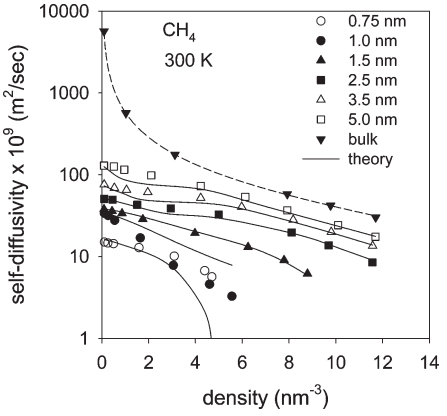

Figure 3. Variation of self-diffusivity with density for CH_4 at 300 K in pores of various sizes. Symbols represent EMD simulation results and solid lines represent the theoretical predictions.

Viscosities were also obtained from the bulk EMD simulations, using the autocorrelation of the stress tensor. Table 3 lists the correlations obtained for the density variation of the bulk viscosity. On the basis of the well-known kinetic theory results for viscosity and self-diffusivity[40] obtained through the Chapman−Enskog solution of the Boltzmann equation, one expects that at sufficiently low densities

$$D_{s0} = \frac{15k_B T}{128\pi\sigma^4\Omega_{11}\Omega_{22}\rho\eta} \quad (26)$$

where Ω_{11} and Ω_{22} are the collision integrals for the viscosity and self-diffusivity, respectively.[40] Figure 2 depicts a plot of self-diffusivity against $15k_BT/(128\pi\sigma^4\Omega_{11}\Omega_{22}\rho\eta)$ based on the EMD results. The collision integrals were estimated from published tables.[57] It is evident that the results for CH_4 collapse

dx.doi.org/10.1021/jp206811a |J. Phys. Chem. B 2011, 115, 11700–11711

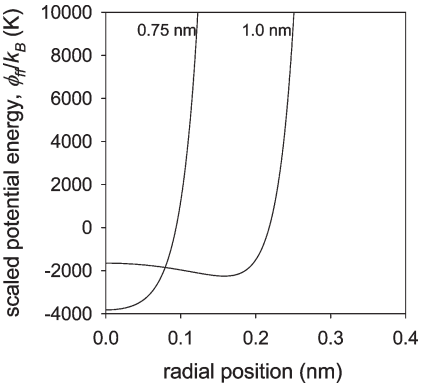

Figure 4. Fluid−solid potential energy profiles for CH_4 in pores of 0.75 and 1.0 nm diameter.

onto a single curve, covering all three temperatures. At low densities, all the results approach the kinetic theory result given by the solid line, as expected. However, as density increases, the data for the different species begin to deviate from each other and the kinetic theory result.

4.2. Self-Diffusion in Nanopores. EMD simulations were next conducted to determine the self-diffusivities of CH_4, CF_4, and CCl_4 at various densities in cylindrical silica pores of different sizes, using the Tjatjopoulos et al.[47] potential in eq 22. Theoretical values of the self-diffusivity were also estimated by the solution of eq 7 using the boundary conditions $dv/dr = 0$ at $r = 0$ and $r = r_p$, discussed above. In obtaining the solution of the velocity profile, eq 7 was formally integrated and converted into an integral equation as in our previous work[37,38] for collective transport. This integral equation was solved using Picard iterations, mixing old and new solutions to promote convergence.

Figure 3 depicts the variation of self-diffusivity with density for CH_4 at 300 K in pores of various diameters, covering both micropores and mesopores. In this figure, the symbols represent the EMD results for which the error is within 5% on the basis of several repeat runs, and the error bars are smaller than the symbol size. As expected, the self-diffusivity decreases with an increase in density, in contrast to the collective diffusivity, which increases with an increase in density.[37,38] However, the self-diffusivity in the pores of different sizes has a weaker dependence on the density than does the bulk fluid, particularly at low density. The solid lines in the figure represent the theoretical predictions, showing excellent agreement with the simulation data for pores of 1.5 nm diameter and larger. At large pore size and high density, the self-diffusivity approaches the bulk value, as expected. It should be noted that the theory is completely predictive, utilizing only data for bulk self-diffusivity and the equilibrium density profiles and has no adjustable parameters.

The results in Figure 3 predict self-diffusivity values at 300 K in the range of 3×10^{-9}−10^{-7} m^2/s for methane in silica pores having a diameter of 0.75−5 nm. For comparison, the experimentally obtained diffusivity of CH_4 at 334 K in silicalite, which has a center−center pore diameter of about 0.63 nm, is in the range of 7×10^{-9}−10^{-8} m^2/s on the basis of NMR data.[7] This is only marginally lower than the theoretical results for the 0.75 nm diameter pore in Figure 3, confirming that the theoretical results are quantitatively in the correct range. A more direct comparison of the oscillator model with experimental results for the diffusion of various gases through a DDR zeolite membrane has been made earlier[24] and has demonstrated the validity of the model.

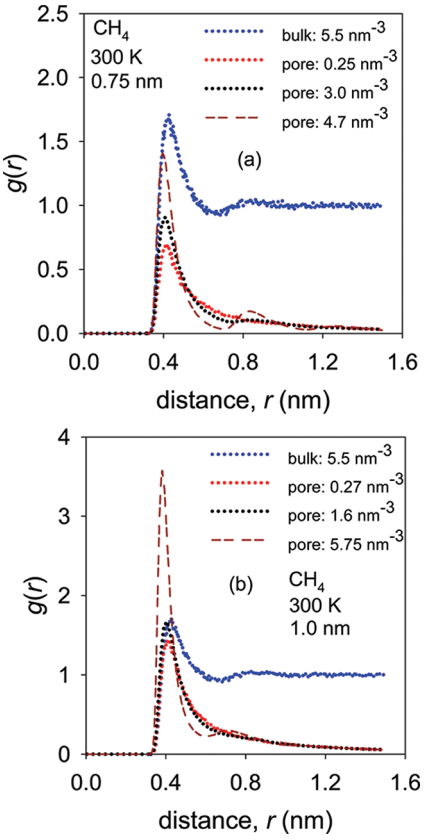

Figure 5. Pair distributions of CH_4 in bulk and pore fluids at 300 K and various densities. Pore diameter is (a) 0.75 nm and (b) 1.0 nm.

It is seen that, for the pores with a diameter of 0.75 and 1.0 nm, there is considerable deviation between the theory and simulation, particularly for the 1.0 nm pore size, except in the low density region where the oscillator model, on which the friction coefficient is based, is exact. This deviation is due to the inapplicability of the bulk-based viscosity in such narrow pores, where the cross-section is not large enough to accommodate more than two molecules. Figure 4 depicts the fluid−solid potential energy profiles in pores of these sizes, showing a potential minimum at the pore center for the 0.75 nm diameter pore, while a weak minimum exists at a radial position of about 0.16 nm for the 1.0 nm diameter pore. Thus, only one molecule can be accommodated in the pore cross-section in the 0.75 nm pore, and the flow is essentially one-dimensional, whereas for the 1.0 nm pore, two molecules can only just be accommodated in the pore. In the latter case, it has been shown[58] that molecules on opposite sides of the pore diameter will hinder each other's radial oscillations, leading to a repulsive core in the pore. Because the bulk viscosity is isotropic, it is representative of the transport properties of a three-dimensional fluid, and its application in such narrow pores, even allowing for the nonuniformity of the adsorbed fluid using the LADM, can be expected to be inaccurate. This will lead to predictive errors in the region where fluid−fluid intermolecular interactions become important. A more accurate theory at such pore sizes may be possible on the basis of the analysis developed earlier[58] for the corrected diffusivity, D_{t0}, and will be addressed in future work.

Figure 5a,b depicts the pair distributions (PDFs) of CH_4 at various densities in the pores with diameters of 0.75 and 1.0 nm,

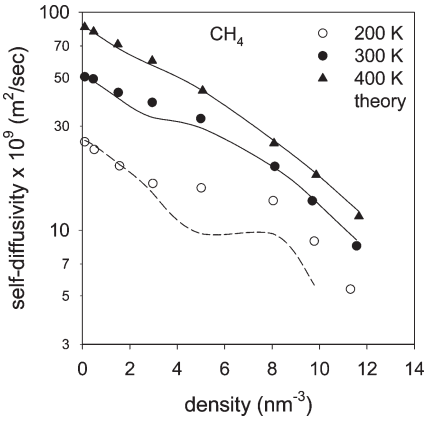

Figure 6. Variation of self-diffusivity with density for CH_4 in pore of 2.5 nm diameter at 200, 300, and 400 K. Symbols represent EMD simulation results, and solid lines represent the theoretical predictions.

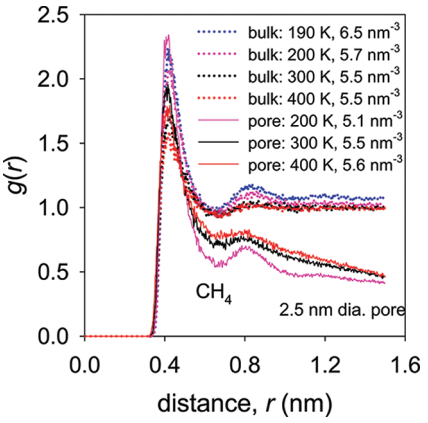

Figure 7. Pair distributions of CH_4 in bulk and pore fluids at various temperatures. Pore diameter is 2.5 nm.

respectively, and for the bulk fluid at a density of 5.5 nm^{-3}, obtained from GCMC simulations. At the pore size of 0.75 nm (Figure 5a), it is seen that the PDFs of the bulk and pore fluid are somewhat similar for densities up to 3.0 nm^{-3}; however, at the higher density of 4.7 nm^{-3}, the PDF of the pore fluid has a significantly sharper first peak and a more prominent second peak compared to the bulk. This is a consequence of the differences in packing between the bulk and pore fluids, resulting in differences in intermolecular interactions and thus in viscous-like effects between the pore and bulk fluids beyond a density of 3.0 nm^{-3} (these are not accounted for in the bulk viscosity used in the LADM). Similarly, for the pore size of 1.0 nm, it is seen that at all densities the PDFs of the pore fluid have a much sharper first peak (Figure 5b) than the PDF for the bulk fluid, implying that the molecules are more strongly caged by their fluid neighbors than in the bulk fluid. This explains the discrepancy between the theory and simulation above a density of 3.0 nm^{-3} in the 0.75 nm pore and above a density of 0.55 nm^{-3} in the 1.0 nm pore. As will be shown subsequently, intermolecular interactions assume significance in the regions where the discrepancy occurs, and the bulk viscosity no longer suffices to account for the effect of fluid−fluid intermolecular collisions in these pores due to the differences in packing (i.e., differences in the PDFs).

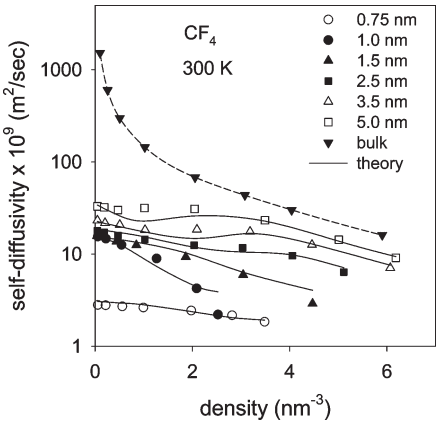

Figure 8. Variation of self-diffusivity with density for CF_4 at 300 K in pores of various sizes. Symbols represent EMD simulation results and solid lines represent the theoretical predictions.

The experimental bulk critical temperature of CH_4 is 190.4 K, and at 300 K it is supercritical. To investigate the behavior near the critical temperature and far from it, EMD simulations were conducted for CH_4 at 200 and 400 K in a pore of 2.5 nm diameter. Figure 6 depicts the EMD results and theoretical predictions based on the solution of eqs 7−14, showing excellent agreement between theory and simulation at 300 and 400 K but not at 200 K, which is close to the bulk critical temperature. In the latter case, the theory underpredicts the self-diffusivity above a density of 3 nm^{-3}, although the qualitative shape of the theoretical D_{s0}/ρ curve matches that of simulation. The discrepancy between the theory and simulation is largest at a density of about 6 nm^{-3}, which is close to the bulk critical density of CH_4 of 6.1 nm^{-3}. The weakness of the theory close to T_c can be traced to inaccuracy in the LADM in eq 3, which averages the fluid density within a sphere of diameter σ_{ff}. Near the critical temperature, the correlation length of a fluid is known to scale as $[(T - T_c)/T_c]^{-\nu}$ and becomes divergent at the critical temperature.[59] Consequently, in the presence of the strong density gradients that exist in nanopores, the averaging within a sphere of diameter σ_{ff} in the LADM will be inaccurate close to T_c. Support for this conclusion is seen from the pair distribution, $g(r)$, of the bulk and pore fluids (for a pore of 2.5 nm diameter) at a density of approximately 5−6 nm^{-3}, depicted in Figure 7. At 190 K, it is seen that the bulk fluid has a strong second peak, which persists even at 200 K. At 300 and 400 K, the bulk as well as pore fluids have only a weak second peak, and its intensity reduces with an increase in temperature. By contrast, the pore fluid has a strong second peak at 200 K, indicative of a longer range of the correlations. This second peak occurs at about 0.8 nm, a distance considerably larger than the hard sphere diameter σ_{ff} (= 0.381 nm for CH_4) over which the LADM averages the density, so that the latter may not be expected to accurately capture the effect of inhomogeneity on the viscosity (i.e., on intermolecular interactions). At 300 and 400 K, where the second peak is very weak, the long-range correlations are insignificant and the LADM assumption may be valid. This is confirmed by the good agreement between simulation and theory for D_{s0} at these temperatures in Figure 5.

Figure 8 depicts the variation of self-diffusivity with density for CF_4 at 300 K in silica pores of various diameters. As for CH_4, excellent agreement is seen between the theory and EMD for pores of diameter 1.5 nm and larger, with the self-diffusivity at

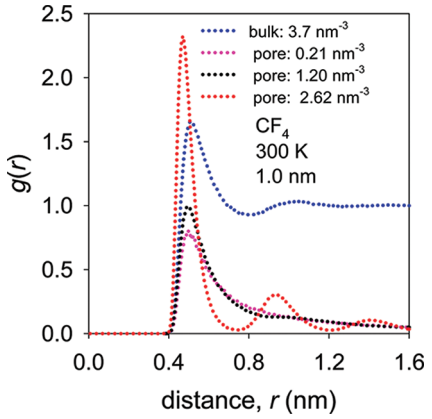

Figure 9. Pair distributions of CF_4 in bulk and pore fluids at 300 K and various densities. Pore diameter is 1.0 nm.

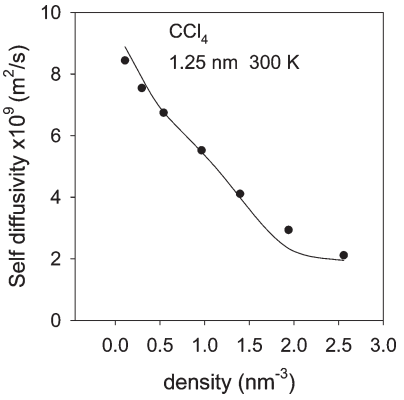

Figure 10. Variation of self-diffusivity with density for CCl_4 at 300 K in a 2.5 nm diameter pore. Symbols represent EMD simulation results and solid line represents the theoretical predictions.

large pore size and high density approaching the bulk value. In such pores, more than two molecules can be accommodated in a cross-section, and the viscosity based on bulk values provides an adequate representation of the frictional interaction between fluid molecules, when used in conjunction with the LADM. However, in contrast to CH_4, excellent agreement is also observed for the pore of diameter 0.75 nm, where the transport is essentially one-dimensional. For the pore diameter of 1.0 nm, the agreement is good at low density but deteriorates above a density of about 1 nm^{-3}. It will be subsequently shown that the good agreement at 0.75 nm pore size is due to the insignificance of intermolecular interactions, whereas these interactions are important above a density of about 1 nm^{-3} in the 1.0 nm pore. The use of the isotropic bulk viscosity to calculate local viscosities at this pore size, therefore, leads to inaccuracy above a density of 1.0 nm^{-3} and to the discrepancy between theory and simulation. Figure 9 depicts the PDF of CF_4 for the bulk fluid at a density of 3.7 nm^{-3} and for that at various densities in the 1.0 nm pore at 300 K. It is seen that the bulk fluid has only a weak second peak and that at a density of 1.2 nm^{-3} and below, the PDF of the pore fluid is similar to that of the bulk. However, at the density of 2.62 nm^{-3}, the PDF of the pore fluid displays a much sharper first peak and significant long-range correlations through the presence of second and third peaks. These long-range correlations

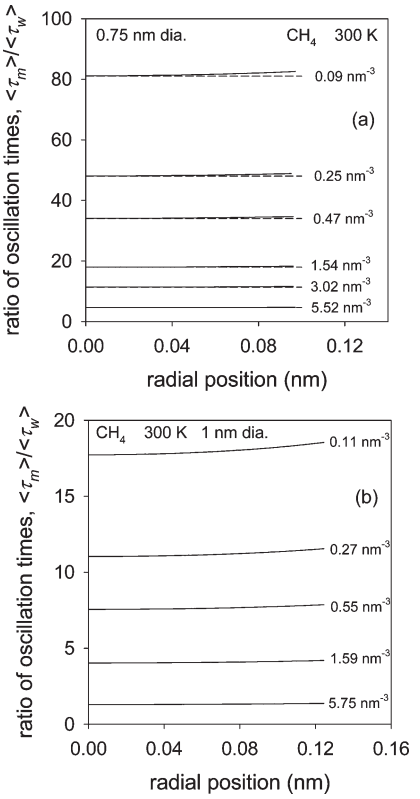

Figure 11. Variation of ratio of oscillation times, $[\tau_m(r)/\langle\tau\rangle]$, with radial position for CH_4 at various densities at 300 K in a pore of (a) 0.75 nm and (b) 1.0 nm diameter. The solid line corresponds to the result from eq 21, and the dashed line in (a) corresponds to that obtained from eq 27.

are absent in the bulk fluid and are therefore not captured through the LADM, leading to the discrepancy between the theoretically predicted and simulation-based self-diffusivities at this pore size.

All of the simulation and theoretical results discussed above have related to systems above the critical temperature of the diffusing fluid. To test the adequacy of the theory at subcritical temperatures, simulations were also conducted for CCl_4 at 300 K in a cylindrical silica pore of 2.5 nm diameter. At this temperature CCl_4 is subcritical, as its critical temperature is 556.3 K. Figure 10 depicts the simulation results and theoretical predictions for the self-diffusivity, showing very good agreement between the two. Some minor deviation occurs at densities in the neighborhood of 2.0 nm^{-3}, which is close to the critical density of CCl_4 of 2.18 nm^{-3}.

The above results indicate some weakness of the theory near the critical point, where the correlation length scale of the fluid diverges but fairly robust behavior at other temperatures and for pore sizes that can accommodate more than two molecules in the cross-section. When the pore size is too small to accommodate more than two molecules in the cross-section, the theory provides accurate estimates of the self-diffusivity for densities small enough that fluid−fluid intermolecular interactions are not significant. In what follows, we demonstrate the utility of the criterion for significance of fluid−fluid intermolecular interactions, developed in Section 2.2.

4.3. Criterion for Importance of Fluid−Fluid Interactions. The inaccuracy in theoretical predictions of self-diffusivity for

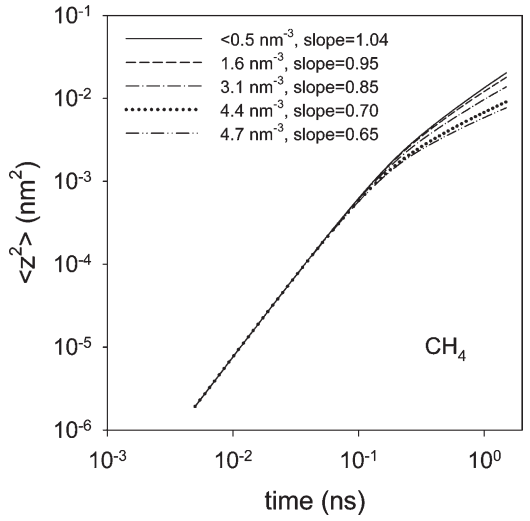

Figure 12. Variation of mean squared displacement with time for CH_4 at 300 K at various densities in a 0.75 nm diameter pore.

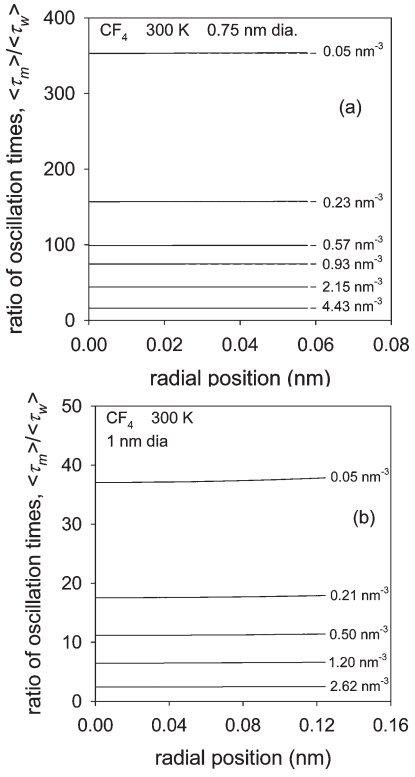

Figure 13. Variation of the ratio of oscillation times, $[\tau_m(r)/\langle\tau\rangle]$, with radial position for CF_4 at various densities at 300 K in a pore of (a) 0.75 nm and (b) 1.0 nm diameter. The solid line corresponds to the result from eq 21, and the dashed line in (a) corresponds to that obtained from eq 27.

CH_4 at 300 K above a density of about 3 nm^{-3} in the nanopore of diameter 0.75 nm and above about 0.5 nm^{-3} in the 1.0 nm diameter pore, as well as for CF_4 above about 1 nm^{-3} in the 1.0 nm pore, has been traced to differences in the packing between the pore and bulk fluids. Confirmation of the importance of fluid−fluid interactions in the region of discrepancy will provide strong support for the effect of differences in the packing.

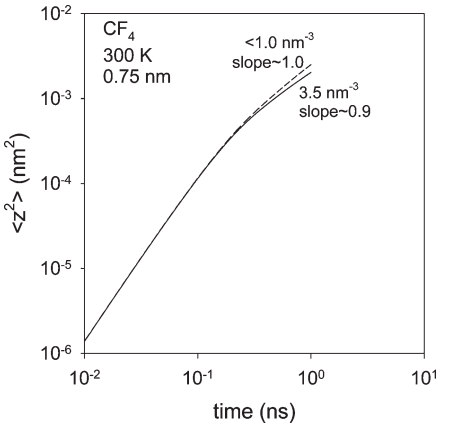

Figure 14. Variation of mean squared displacement with time for CF_4 at 300 K at various densities in a 1.0 nm diameter pore.

Fluid−fluid interactions will not have significant influence when the mean axial oscillation time, $\tau_m(r)$, of a molecule in the interaction field due to the other fluid molecules, determined by eq 21, is much larger than its oscillation time, $\langle\tau\rangle$, in the fluid−solid interaction field. Conversely, taking an order of magnitude as defining "much larger than", we may consider fluid−fluid interactions to be important when $[\tau_m(r)/\langle\tau\rangle] < 10$.

Figure 11a,b depicts the variation of the ratio of oscillation times, $[\tau_m(r)/\langle\tau\rangle]$, with radial position for CH_4 at various densities in a pore of 0.75 and 1.0 nm diameter, respectively. It is found that the profiles are relatively flat, and the ratio of oscillation times varies only weakly with position. At the pore diameter of 0.75 nm, the ratio is in the range of 11.4−11.6 at a density of 3.0 nm^{-3} and is larger at lower densities. Thus, fluid−fluid interactions will assume significance above a density of about 3 nm^{-3} at this pore size. Similarly, for the pore diameter of 1.0 nm, the ratio is in the range 11.0−11.6 at a density of 0.27 nm^{-3} and is larger for lower densities. Thus, at this pore size, fluid−fluid interactions are important above a density of about 0.27 nm^{-3}. These regions of significance of fluid−fluid interactions are precisely the regions of discrepancy between theory and simulation reported above and support the explanation of the weakness in the use of the bulk-based viscosity in the LADM at these narrow pore sizes, where less than two molecules can be accommodated in the pore cross-section.

CH_4 has a potential minimum at the center in the pore of 0.75 nm diameter (c.f., Figure 4), and only one CH_4 molecule can fit in the cross-section. In this pore, one expects nearly one-dimensional motion, and if this assumption is enforced, eq 21 simplifies to

$$\tau_m = \frac{\sqrt{2\pi m}}{r_p\left(\langle\rho\rangle\int_0^{\infty}\int_0^{2\pi}\int_0^{r_p}\left(\frac{d^2\phi_{ff}}{dz^2}\right)_{eq} g(z)\, dz\right)^{1/2}} \qquad (27)$$

The dashed line in Figure 11a corresponds to the ratio of oscillation times when the value of τ_m is estimated using eq 27. This matches quite well with the more exact result obtained using eq 21 for $\tau_m(r)$, confirming that for the pore size of 0.75 nm, the molecular motion is essentially one-dimensional. In such pores, single file motion occurs, and it is known[60] that when intermolecular interactions are significant, self-diffusion is nonclassical,

and the mean squared molecular displacement displays long-time behavior $\langle z^2 \rangle \propto \sqrt{t}$. This behavior is frequently referred to as single-file diffusion.[60] Figure 12 depicts the variation of $\langle z^2 \rangle$ with t on logarithmic coordinates for CH_4 in the 0.75 nm diameter pore, showing the slope at long-time to gradually decrease from unity, which is symptomatic of significant intermolecular interactions. At a density of about 3 nm^{-3} the slope is 0.85, and the self-diffusion is nearly classical, but at higher densities the slope rapidly decreases toward the single file asymptote, again confirming the significance of intermolecular interactions above a density of about 3.0 nm^{-3}.

Figure 13a,b depicts the variation of oscillation time ratio for CF_4 in a 0.75 and 1.0 nm diameter pore, respectively. The excellent agreement of the dashed lines based on eq 27 with the results based on eq 21 in Figure 13a also confirms the one-dimensional nature of the CF_4 for this pore size. For the 0.75 nm diameter pore, the ratio exceeds 10 at all densities investigated and is about 16.2 at a density of 4.43 nm^{-3}. Thus, intermolecular fluid−fluid interactions are insignificant over the range of densities investigated. This explains the good agreement of the theory and simulations for this pore size in Figure 8. In confirmation, Figure 14 shows that the slope of the mean squared deviation versus time plot is above 0.9 over the entire range of densities investigated in Figure 8, so that intermolecular interactions are of negligible influence, and normal Fickian diffusion holds. Figure 13b shows that one may expect the theory developed here to be inaccurate for CF_4 above a density of about 0.5 nm^{-3} in a 1.0 nm diameter pore, as the ratio of oscillation times then becomes smaller than 10 and fluid−fluid interactions assume significance. This is in agreement with the results in Figure 8 for the 1.0 nm pore, in which less than two molecules can fit in the cross-section and the bulk-based viscosity embedded in the LADM will not adequately represent the effect of the fluid−fluid interactions.

5. CONCLUSIONS

The self-diffusion of simple Lennard-Jones fluids in cylindrical silica nanopores has been investigated here, both theoretically and using simulation. It is found that the self-diffusivity in the pores has a considerably weaker decline with an increase in density, particularly at low density where the effect of the confining walls dominates. Our recent friction-based theory of transport in nanopores, originally developed for predicting the collective diffusion coefficient, has been extended here to predict the self-diffusivity. It is found that the theory performs well over a wide range of pore sizes, despite the absence of any fitting parameters. Exceptions are found at temperatures near the critical point and in molecularly narrow pores at densities where the fluid−fluid intermolecular interactions become significant. By considering the oscillations of a fluid molecule slightly perturbed from its equilibrium position within the force field of the surrounding molecules, we have formulated a criterion to determine the conditions when intermolecular interactions are important in the transport. The criterion considers the ratio of oscillation times in the force field of the surrounding particles and that of the pore wall and is seen to correlate very well with the region of discrepancy between theory and simulation found for the molecularly narrow pores. In such pores, the nonuniform viscosity derived from bulk fluid data used in the theory cannot effectively capture the effect of intermolecular interactions, and this leads to the inaccuracies in these circumstances.

AUTHOR INFORMATION

Corresponding Author
*E-mail: s.bhatia@uq.edu.au.

ACKNOWLEDGMENT

This research has been supported by a Discovery grant from the Australian Research Council. One of us (S.K.B.) acknowledges an Australian Professorial Fellowship from the Australian Researches Council. We thank the High Performance Computing Unit of the University of Queensland for access to supercomputing facilities.

REFERENCES

(1) Bhatia, S. K.; Bonilla, M. R.; Nicholson, D. *Phys. Chem. Chem. Phys.* **2011**, *13*, 15350–15383.
(2) Rafii-Tabar, H. *Phys. Lett.* **2004**, *390*, 235–242.
(3) Selvam, P.; Bhatia, S. K.; Sonwane, C. G. *Ind. Eng. Chem. Res.* **2001**, *40*, 3237–3261.
(4) Rosi, N. L.; Eckert, J.; Eddaoudi, M.; Vodak, D. T.; Kim, J.; O'Keeffe, M.; Yaghi, O. M. *Science* **2003**, *300*, 1127–1129.
(5) Eijkel, J. C. T.; van den Berg, A. *Microfluid. Nanofluid.* **2005**, *1*, 249–267.
(6) Sansom, M. S. P.; Biggin, P. C. *Nature* **2001**, *414*, 156–159.
(7) Kärger, J.; Ruthven, D. M. *Diffusion in Zeolites and Other Microporous Solids*; John Wiley: New York, 1992.
(8) Nicholson, D.; Travis, K. In *Recent Advances in Gas Separation by Microporous Membranes*; Kanellopoulos, N., Ed.; Elsevier: Amsterdam, 2000.
(9) Bhatia, S. K.; Nicholson, D. *Phys. Rev. Lett.* **2003**, *90*, 016105.
(10) Bhatia, S. K.; Nicholson, D. *J. Chem. Phys.* **2003**, *119*, 1719–1730.
(11) MacElroy, J. M. D.; Suh, S. H. *Microporous Mesoporous Mater.* **2001**, *48*, 195–202.
(12) MacElroy, J. M. D.; Pozhar, L. A.; Suh, S. H. *Colloids Surf., A* **2001**, *187*, 493–507.
(13) Kharat, P.; Krishnan, S. H.; Ayappa, K. G. *Mol. Phys.* **2006**, *104*, 3809–3819.
(14) Dvoyashkin, M.; Valiullin, R.; Kärger, J.; Einicke, W.-D.; Gläser, R. *J. Am. Chem. Soc.* **2007**, *129*, 10344–10345.
(15) Kärger, J.; Freude, D. *Chem. Eng. Technol.* **2002**, *25*, 769–778.
(16) Dvoyashkin, M.; Valiullin, R.; Kärger, J. *Adsorption* **2007**, *13*, 197–200.
(17) Valiullin, R.; Kärger, J.; Gläser, R. *Phys. Chem. Chem. Phys.* **2009**, *11*, 2833–2853.
(18) Coppens, M.-O.; Bell, A. T.; Chakraborty, A. K. *Chem. Eng. Sci.* **1999**, *53*, 2053–2061.
(19) Malek, K.; Coppens, M.-O. *Phys. Rev. Lett.* **2001**, *12*, 125505.
(20) Coppens, M.-O.; Dammers, A. J. *Fluid Phase Equilib.* **2006**, *241*, 308–316.
(21) Mason, E. A.; Malinauskas, A. P. *Gas Transport in Porous Media: The Dusty-Gas Model*; Elsevier: Amsterdam, 1983.
(22) Jepps, O. G.; Bhatia, S. K.; Searles, D. J. *Phys. Rev. Lett.* **2003**, *91*, 0126102.
(23) Bhatia, S. K.; Jepps, O. G.; Nicholson, D. *J. Chem. Phys.* **2004**, *120*, 4472–4485.
(24) Bhatia, S. K. *Langmuir* **2010**, *26*, 8373–8385.
(25) Bhatia, S. K.; Nicholson, D. *Chem. Eng. Sci.* **2010**, *65*, 4519–4520.
(26) Krishna, R.; van Baten, J. M. *J. Membr. Sci.* **2011**, *377*, 249–260.
(27) Krishna, R.; van Baten, J. M. *Chem. Eng. Sci.* **2009**, *64*, 3159–3178.
(28) Krishna, R. *Chem. Eng. Sci.* **1990**, *45*, 1779–1791.
(29) Krishna, R. *Chem. Eng. Sci.* **1993**, *48*, 845–861.

(30) Davis, H. T. In *Fundamentals of Inhomogeneous Fluids*; Henderson, D., Ed.;Marcel Dekker: New York, 1992.
(31) Pozhar, L. A.; Gubbins, K. E. *Int. J. Thermophys.* **1999**, *20*, 805–813.
(32) Pozhar, L. A. *Transport Theory of Inhomogeneous Fluids*; World Scientific: Singapore, 1994.
(33) Guo, Z.; Zhao, T. S.; Shi, Y. *Phys. Rev. E: Stat., Nonlinear, Soft Matter Phys.* **2005**, *71*, 035301.
(34) Guo, Z.; Zhao, T. S.; Xu, C.; Shi, Y. *Int. J. Comput. Fluid Dyn.* **2006**, *20*, 361–367.
(35) Marconi, U. M. B.; Melchionna, S. *J. Chem. Phys.* **2011**, *134*, 064118.
(36) Bhatnagar, P. L.; Gross, E. P.; Krook, M. *Phys. Rev.* **1954**, *94*, 511–525.
(37) Bhatia, S. K.; Nicholson, D. *J. Chem. Phys.* **2008**, *129*, 164709.
(38) Bhatia, S. K.; Nicholson, D. *Phys. Rev. Lett.* **2008**, *100*, 236103.
(39) Bearman, R. J.; Kirkwood, J. G. *J. Chem. Phys.* **1958**, *28*, 136–145.
(40) McQuarrie, D. A. *Statistical Mechanics*; University Science: Sausalito, CA, 2000.
(41) Kerkhof, P. J. A. M.; Geboers, M. A. M. *AIChE J.* **2005**, *51*, 79–121.
(42) Travis, K. P.; Todd, B. D.; Evans, D. J. *Phys. Rev. E: Stat., Nonlinear, Soft Matter Phys.* **1997**, *55*, 4288–4295.
(43) Bitsanis, I.; Magda, J. J.; Tirrell, M.; Davis, H. T. *J. Chem. Phys.* **1987**, *87*, 1733–1750.
(44) Reis, R. A.; Nobrega, R.; Oliveira, J. V.; Tavares, F. W. *Chem. Eng. Sci.* **2005**, *60*, 4581–4592.
(45) Dariva, C.; Coelho, L. A. F.; Oliveira, J. V. *Braz. J. Chem. Eng.* **1999**, *16*, 213–227.
(46) Kerkhof, P. J. M. *Chem. Eng. J.* **1996**, *64*, 319–343.
(47) Tjatjopoulos, G. J.; Feke, D. L.; Mann, J. A. *J. Phys. Chem.* **1988**, *92*, 4006–4007.
(48) Neimark, A. V.; Ravikovitch, P. I.; Grun, M.; Schuth, M. F.; Unger, K. K. *J. Colloid Interface Sci.* **1998**, *207*, 159–169.
(49) Adams, D. J. *Mol. Phys.* **1974**, *28*, 1241–1252.
(50) Metropolis, N.; Rosenbluth, A. W.; Rosenbuth, M. N.; Teller, A. N.; Teller, E. *J. Chem. Phys.* **1953**, *21*, 1087–1092.
(51) Evans, D. J.; Morriss, G. P. *Statistical Mechanics of Nonequilibrium Liquids*; Academic Press: London, 1990.
(52) Dubbeldam, D.; Snurr, R. Q. *Mol. Sim.* **2007**, *33*, 305–325.
(53) Sokhan, V. P.; Nicholson, D.; Quirke, N. *J. Chem. Phys.* **2002**, *117*, 8531–8539.
(54) Chen, H. B.; Sholl, D. S. *J. Am. Chem. Soc.* **2004**, *126*, 7778–7779.
(55) Bhatia, S. K.; Chen, H. B.; Sholl, D. S. *Mol. Simul.* **2005**, *31*, 643–649.
(56) Roth, M. W.; Mesentseva, J. *Mol. Simul.* **2004**, *30*, 661–667.
(57) Bird, R. B.; Stewart, W. E.; Lightfoot, E. N. *Transport Phenomena*; John Wiley: New York, 2002.
(58) Bhatia, S. K.; Nicholson, D. *J. Chem. Phys.* **2007**, *127*, 124701.
(59) Sullivan, D. M.; Neilson, G. W.; Fischer, H. E. *J. Phys.: Condens. Matter* **2000**, *12*, 3531–3542.
(60) Mon, K. K.; Percus, J. K. *J. Chem. Phys.* **2002**, *117*, 2289–2292.